Observed near-surface flows under all tropical cyclone intensity levels using drifters in the northwestern Pacific

Yu-Chia Chang,[1,2] Guan-Yu Chen,[1,2] Ruo-Shan Tseng,[1,2] Luca R. Centurioni,[3] and Peter C. Chu[4]

Received 16 October 2012; revised 19 February 2013; accepted 31 March 2013; published 9 May 2013.

[1] Data from drifters of the surface velocity program and tropical cyclones (TCs) of the Joint Typhoon Warning Center during 1985–2009 were analyzed to demonstrate strong currents under various storm intensities such as category-4 to −5, category-2 to −3, and tropical storm to category-1 TCs in the northwestern Pacific. Current speeds over 2.0 m s^{-1} are observed under major TCs with the strongest mean currents to the right of the storm track. This study provides the characterization of the near-surface velocity response to all recorded TCs, and agrees roughly with Geisler's theory (1970). Our observations also verify earlier modeling results of Price (1983).

Citation: Chang, Y.-C., G.-Y. Chen, R.-S. Tseng, L. R. Centurioni, and P. C. Chu (2013), Observed near-surface flows under all tropical cyclone intensity levels using drifters in the northwestern Pacific, *J. Geophys. Res. Oceans*, *118*, 2367–2377, doi:10.1002/jgrc.20187.

1. Introduction

[2] Oceanic response to tropical cyclones (TCs) has attracted much attention due to its importance for environmental and ecological protection. Many studies have been conducted on the upper ocean cooling, strong ocean currents, and the enhanced ocean primary production triggered by TCs [*O'Brien and Reid*, 1967; *Price et al.*, 1994; *Chu et al.*, 2000; *Lin et al.*, 2003a, 2003b; *Sriver and Huber*, 2007]. Under storms, energy transfer from atmosphere to ocean generally generates surface waves, near-inertial waves, and currents [*Price*, 1983; Price et al., 1994; *D'Asaro*, 1985; *Nilsson*, 1995; *Wunsch*, 1998; *Alford*, 2001, 2003; *Wang and Huang*, 2004; *Liu et al.*, 2008; *Jaimes and Shay*, 2010].

[3] Due to the destructiveness of the TCs, in situ measurements of currents under TCs are not easy, usually with a chance-encountered nature. Despite such difficulty, moored or bottom-mounted current meters sometimes record the ocean currents fortuitously during TC passage. Strong currents (>2.0 m s^{-1}) were measured on the shelf and slope by an array of 14 acoustic Doppler current profilers during the Hurricane Ivan passing through the northeastern Gulf of Mexico in 2004 [*Mitchell et al.*, 2005; *Teague et al.*, 2007]. The observed current structure (high spatial resolution) on the shelf satisfies the Ekman dynamics with stronger currents and transports to the left of the center and with overlapping surface and bottom boundary layers due to topographical constraints. *Zheng et al.* [2006] analyzed the data set of currents collected by two long-term National Oceanic and Atmospheric Administration (NOAA)-moored buoys in the Gulf of Mexico and found almost immediate ocean response at the shelf-break to the passage of a hurricane.

[4] Direct current measurements under TCs during their passage have also been conducted, with deploying airborne expendable current profilers (AXCPs), drifting buoys [*Price et al.*, 1994; *Jacob and Shay*, 2003; *Jaimes and Shay*, 2009], profiling electromagnetic autonomous profiling explorer (EM-APEX) floats [*Sanford et al.*, 2011] ahead of hurricanes. Strong rightward biased currents in mixed layer, ranging from 0.8 to 1.7 m s^{-1}, were identified [*Price et al.*, 1994] from 15 AXCPs under three moving hurricanes with various intensities. Storm-generated surface velocity, with superimposed inertia-gravity-wave motions, reached a maximum speed >1.2 m s^{-1} immediately following the storm passage from three air-dropped drifting buoys ahead of Hurricane Josephine [*Black et al.*, 1988]. Near-inertial currents in the post-TC relaxation stage (about several days) have also been recorded [*Shay and Elsberry*, 1987; *Brink*, 1989; *Price et al.*, 1994; *Teague et al.*, 2007]. Clockwise-rotating currents with near-inertial period and amplitude of 1.5 m s^{-1} in the surface layer were observed from three EM-APEX floats [*Sanford et al.*, 2011] under strong temporally varying surface winds from intensified stage of Hurricane Frances. After analyzing the surface velocity program (SVP) [*Niiler*, 2001] drifter data drogued at 15 m depth in the Taiwan Strait and the Pacific Ocean during the passage of Typhoon Hai-Tang in 2005 and Typhoon Shan-Shan in 2006, an unusual phenomenon of storm-generated flow reversal (maximum current speeds: 1.7–2.0 m s^{-1}) was observed in the Taiwan Strait, with decreasing northward Kuroshio speeds in the western Pacific Ocean [*Chang et al.*, 2010].

[5] After investigating the response of a two-layer ocean to a moving hurricane, *Geisler* [1970] proposed an important

[1]Institute of Applied Marine Physics and Undersea Technology, National Sun Yat-Sen University, Kaohsiung, Taiwan.
[2]Asia-Pacific Ocean Research Center, National Sun Yat-Sen University, Kaohsiung, Taiwan.
[3]Scripps Institution of Oceanography, University of California San Diego, La Jolla, California, USA.
[4]Naval Ocean Analysis and Prediction Laboratory, Department of Oceanography, Naval Postgraduate School, Monterey, California, USA.

Corresponding author: G.-Y. Chen, Institute of Applied Marine Physics and Undersea Technology, National Sun Yat-Sen University, Kaohsiung 804, Taiwan. (guanyu@faculty.nsysu.edu.tw)

2169-9275/13/10.1002/jgrc.20187

theory that inertial-gravity waves are the dominant feature of the upper ocean if the TC's the translation speed U_h exceeds the phase speed of the first baroclinic mode c_1. As $U_h < c_1$ (i.e., the Froude number, $F_r = U_h/c_I < 1$), the oceanic response is a barotropic, geostrophical, and cyclonic gyre with upwelling in the storm's center [*Chang and Anthes*, 1978; *Chang*, 1985; *Ginis and Sutyrin*, 1995]. If $U_h > c_1$ ($F_r > 1$), the currents in the wake become more near inertial after the first half inertial period (P_I). The along-track horizontal scale (L) of wake is proportional to the production of P_I and U_h [*Geisler*, 1970; *Greatbatch*, 1984],

$$L = \alpha P_I U_h, \qquad (1)$$

where α is the proportionality. The initial horizontal scales of TC's wake are directly determined by the scales of the atmospheric forcing [*Garrett and Munk*, 1972; *Gill*, 1984; *Shay and Chang*, 1997]. The ocean mixed-layer (OML) currents in TC's wake cross-track are mainly determined by the wind stress with maximum current speed to the right of the storm track at $y = 2R_{\max}$, where $R_{\max}$ is the radius of the maximum tangential velocity of the storm [*Brooks*, 1983]. For typical storm sizes and translation speeds, the rate of wind stress turning is $O(f)$ [*Price*, 1983]. Thus, wind stress of a moving TC is near-resonant coupling to the OML velocity on the right side of the track, and very poorly coupled on the left side. Furthermore, observed near-inertial currents display smaller horizontal scales due to the local background flow or vorticity. Background-divergent flow dampens near-inertial motions, and background vorticity changes the frequency of the inertial response and current structure [*Mooers*, 1975; *Olbers*, 1981; *Weller*, 1982; *Gill*, 1984; *Kunze*, 1985; *Shay et al.*, 1989; *Jaimes and Shay*, 2010].

[6] Up until now, the direct velocity measurements from individual storms were used to characterize the horizontal structure in the wake of some individual storms. Although the *Geisler*'s [1970], classical linear theory was incorporated in modeling studies for upper ocean response to a moving TC, no statistically significant verification has been conducted on the theory with direct velocity measurements for a relatively long time period. Questions arise: What are the characteristics of near-surface currents to TCs with all intensity-levels from direct velocity measurements? Can the observations verify earlier modeling results of *Price* [1983]? The goal of this study is to answer these questions. To do so, the SVP drifter data of 1985–2009 for the northwestern Pacific are used to represent the observed upper ocean currents under all recorded TCs. Rest of the paper is organized as follows. Description of data and method of removing the preexisting background flow from altimetry-based sea surface height composites are presented in section 2. Mean near-surface flows under major and minor TCs are shown in section 3. Results are discussed with a focus on the evaluation of the earlier modeling results in section 4. Summary are presented in section 5.

2. Data and Method

[7] TC occurrence with 6 h temporal resolution during 1985–2009 was acquired from the best track data from the Joint Typhoon Warning Center (http://metocph.nmci.navy.mil/jtwc.php). Upper ocean current velocities (also with 6-h resolution) were from SVP with drifters drogued at a nominal depth of 15 m (from the website: http://www.aoml.noaa.gov/phod/dac/dacdata.php). The estimated accuracy of the velocity measurements using SVP drifters in a 10 m s^{-1} wind is 10^{-2} m s^{-1} [*Niiler et al.*, 1995]. The tracks of TCs and ocean SVP drifter locations are presented during 1985–2009 in the northwestern Pacific from 10° to 30°N and 100° to 170°E with various intensities based on the Saffir-Simpson Scale, such as category-4 to −5 (Figure 1a), category-2 to −3 (Figure 1b), and tropical storm (TS) to category-1 (Figure 1c) with corresponding numbers of six hourly locations of (centers of TCs, SVP drifters): (1475, 3528), (2374, 4611), and (8004, 11056). The relative locations and distances between storm center and SVP drifter were estimated as the universal time coordinated (UTC) storm and SVP drifter at the same time.

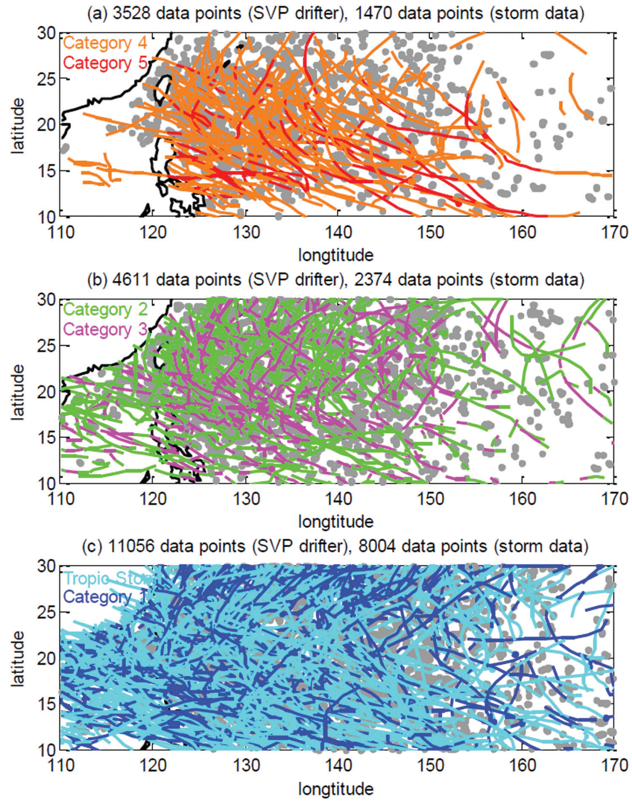

Figure 1. (a) Category-4 and −5, (b) category-2 and −3, and (c) tropical storm and category-1 TCs' tracks and data points of NOAA/AOML SVP drifters (gray dots) in the northwestern Pacific during 1985–2009.

[8] The SVP drifter velocity represents the vertically average motion (u, v) in a surface layer of scaling thickness l. This motion is decomposed into geostrophic (u_g, v_g) and ageostrophic (u_e, v_e) components: $\boldsymbol{U} = \boldsymbol{U_g} + \boldsymbol{U_e}$. Here, the complex form is used,

$$\boldsymbol{U} = u + iv, \boldsymbol{U_g} = u_g + iv_g, \boldsymbol{U_e} = u_e + iv_e, i = \sqrt{-1}. \qquad (2)$$

[9] It is noted that $\boldsymbol{U_g}$ is solely determined from the sea surface height. The ageostrophic flow $\boldsymbol{U_e}\left(= \boldsymbol{U} - \boldsymbol{U_g}\right)$ is the difference of the drifter-measured velocity $\boldsymbol{U}$ and the

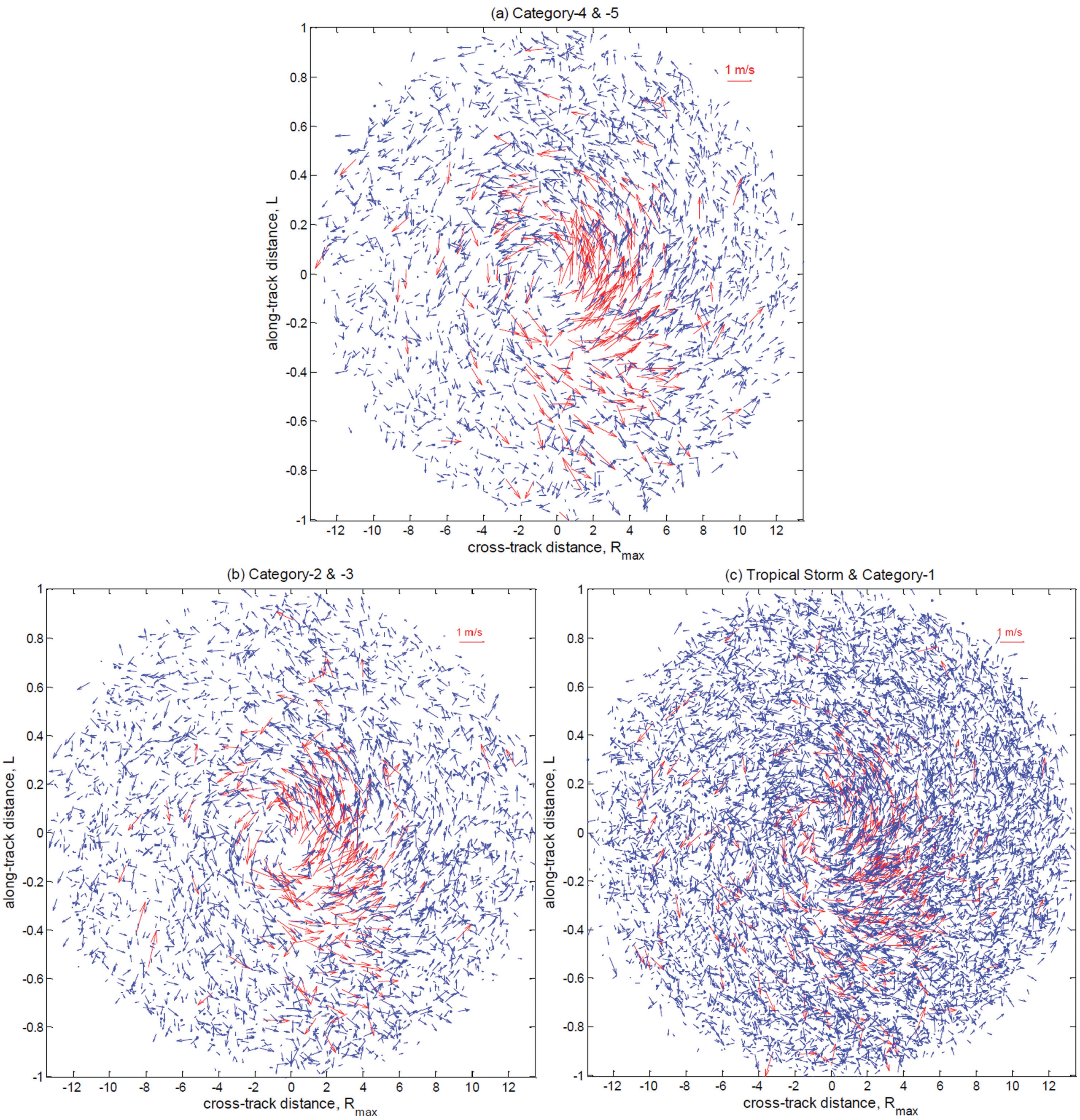

Figure 2. Storm center of (a) category-4 and −5 (2654 data points), (b) category-2 and −3 (3353 data points), (c) tropical storm and category-1 (7997 data points) TCs versus observed current vectors (m s^{-1}) after removing background flow along all TCs' tracks.

geostrophic flow $\boldsymbol{U_g}$ that can be computed from the altimetry-based sea surface height. The equilibrium sea surface height is obtained from 6-year along-track mean computed exclusively from TOPEX/POSEIDON data (1993–1998). The sea surface height during typhoon passage is obtained from multiple altimeter data set with 1/3° × 1/3° horizontal resolution from the Archiving Validation and Interpretation of Satellite data in Oceanography (AVISO), which consists of four satellites (TOPEX/POSEIDON, ERS-1/2, Jason-1, and Geosat-Follow-On) during 1993–2009. The altimetry data are interpolated at each drifter location. Then, the data points of SVP drifter with colocated data reduce to 2654, 3353, and 7997 under category-4 and −5, category-2 and −3, and TS and category-1 TCs, respectively. AVISO sea surface height data are averaged over ~100 km and a week or longer. Thus, knowledge of its inherent uncertainty about small length-scale (e.g., small-scale eddy) and short timescale (e.g., tidal components) errors is necessary before using AVISO altimetry data.

3. Result

[10] In order to obtain statistical relationship between $\boldsymbol{U_e}\left(= \boldsymbol{U} - \boldsymbol{U_g}\right)$ and the TC, the Cartesian coordinate is

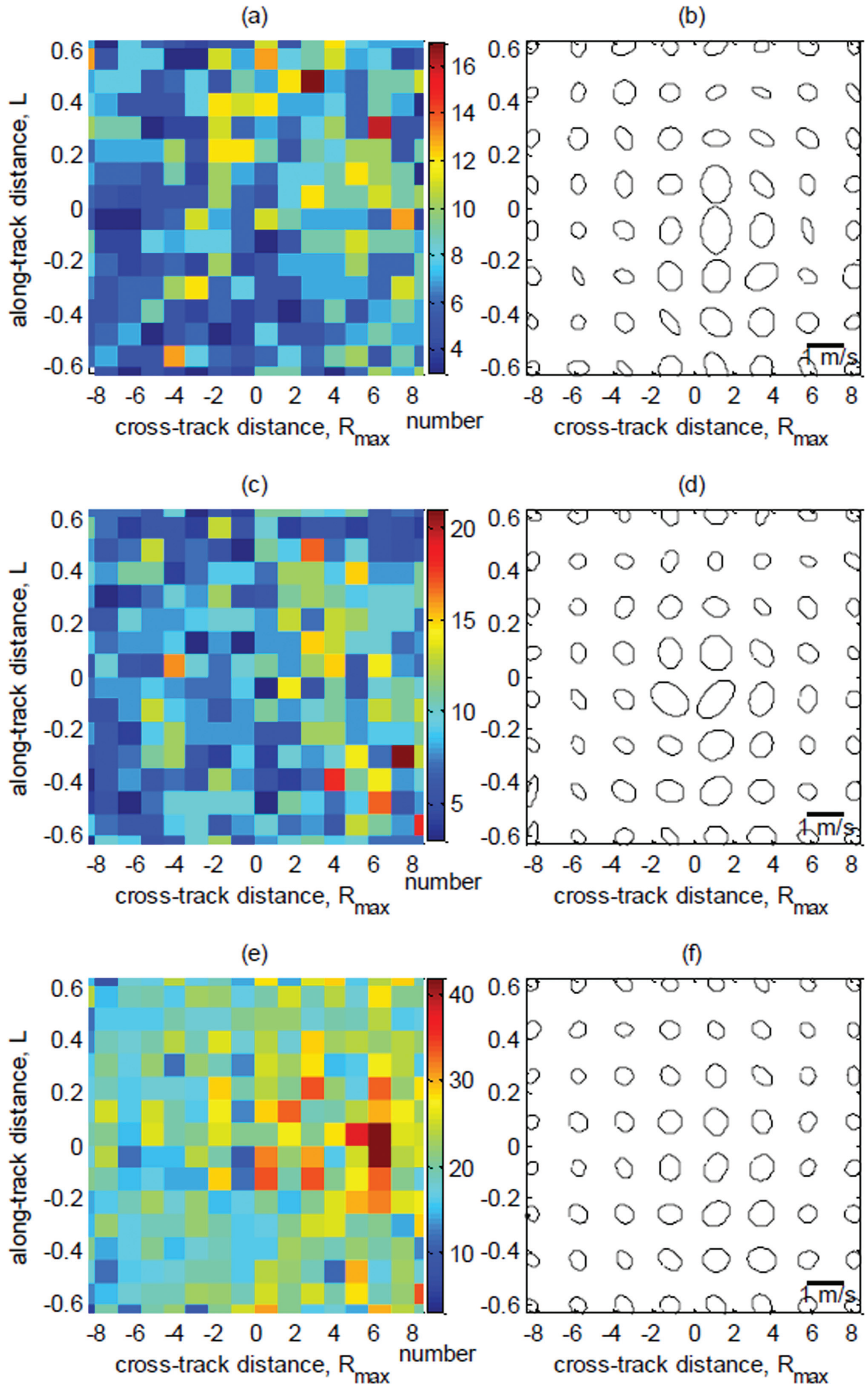

Figure 3. Numbers of data point and their standard error ellipses (m s^{-1}) under (a, b) category-4 and −5, (c, d) category-2 and −3, and (e, f) tropical storm and category-1 TCs.

rotated an angle of φ into the storm-coordinate system with the unit vectors ($\boldsymbol{e}_1$, $\boldsymbol{e}_2$) in the along-track and cross-track directions,

$$\boldsymbol{U}_1 = e^{i\varphi}\boldsymbol{U}_e, \boldsymbol{U}_1 = u_1 + iv_1. \tag{3}$$

[11] Figure 2 shows all observed ocean current vectors ($\boldsymbol{U}_1$) from drifters within the cross-track distance of $13R_{max}$ (~390–780 km typically; if 30 km < R_{max} < 60 km, mean R_{max} = 47 km from *Hsu and Yana* [1998]) and within the along-track distance of L (~260–700 km typically, if 3 m s^{-1} < U_h < 7 m s^{-1}, 24 h < P_I < 28 h), which is the wake's horizontal scale [see equation (1)]. In category-4 and −5 TCs, strong currents (>2.0 m s^{-1}) occurred on the right side of the storm center (Figure 2). Many observed current vectors, which are larger than 0.8 m s^{-1} (red arrows), were located to the right of the path of the storm center under all TCs.

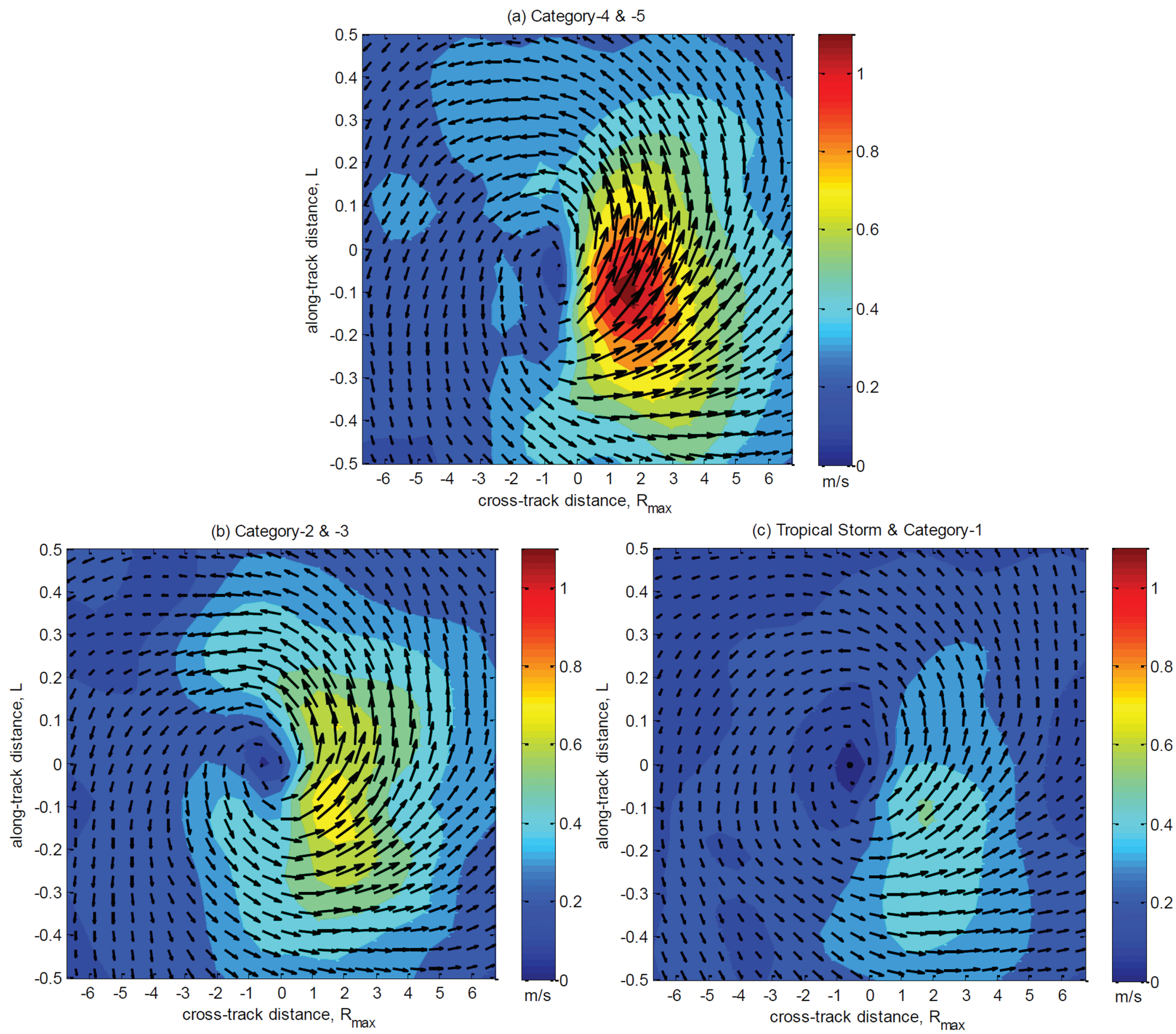

Figure 4. Mean current vectors (m s^{-1}) under (a) category-4 and −5, (b) category-2 and −3, and (c) tropical storm and category-1 TCs. Contour interval is 0.1 m s^{-1}.

[12] In order to display the 2-D current field at all TC intensity levels, these flow vectors were processed by the ensemble average method [*Freeland*, 1975; *Centurioni and Niiler*, 2003; *Centurioni et al.*, 2004; *Lee and Niiler*, 2005]. Figure 3 shows the number of independent observations of SVP drifters and their standard error ellipses. The standard deviations provide error estimates in the reference axis directions. The standard error ellipses show the direction of error of the velocity fluctuations along the major and minor principal axes. The principal angles θ are found from the transcendental relation

$$\tan(2\theta) = \frac{\overline{2u_1'v_1'}}{\overline{u_1'^2} - \overline{v_1'^2}}, \tag{4}$$

where the principal angle is defined for the range $-\pi/2 \le \theta \le \pi/2$ [*Freeland*, 1975]. $\overline{u_1'^2}$ and $\overline{v_1'^2}$ are the major and minor deviation variances in the storm-coordinate system. The lengths of the semiaxes a and b of the standard error ellipse are found as

$$\left\langle {a \atop b} \right\rangle = \sqrt{\frac{1}{2}\left\{\left(\overline{u_1'^2} + \overline{v_1'^2}\right) \pm \left[4\left(\overline{u_1'v_1'}\right)^2 + \left(\overline{u_1'^2} - \overline{v_1'^2}\right)^2\right]^{\frac{1}{2}}\right\}}, \tag{5}$$

in which the sign (+) is used for a and the sign (−) is used for b. In the Pacific, there are rarely direct surface wind data available in TCs. Even in the Atlantic with operational aircraft reconnaissance, surface wind data are actually the exception rather than the rule. Thus, the estimate of R_{max} is usually very rough. Knowledge of its inherent uncertainty (i.e., main error in the principal standard deviations) is needed before compositing observational currents under many storms. Besides, the tidal currents also cause errors. Figures 4a–4c show the mean observed current vectors under

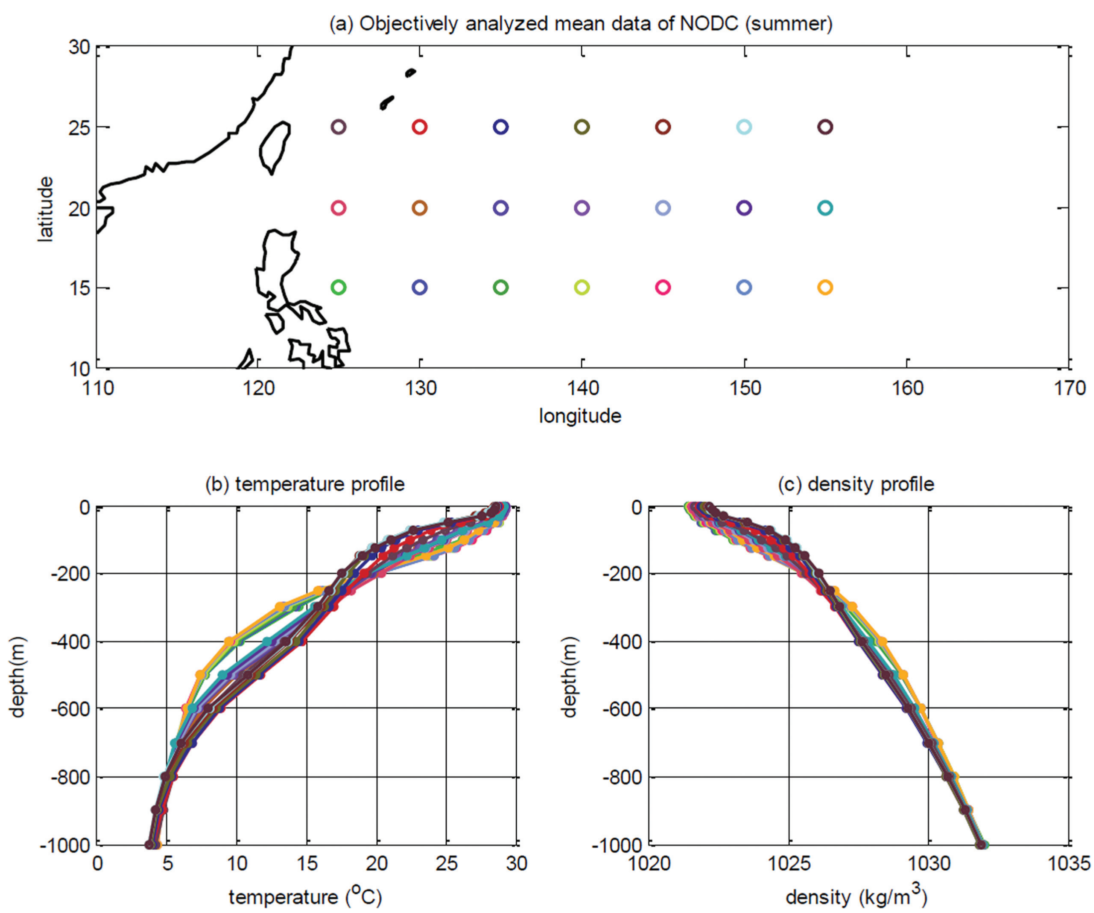

Figure 5. (a) Locations, (b) temperature (°C), and (c) density profiles (kg m^{-3}) of NODC objectively analyzed mean data in the northwestern Pacific during summer.

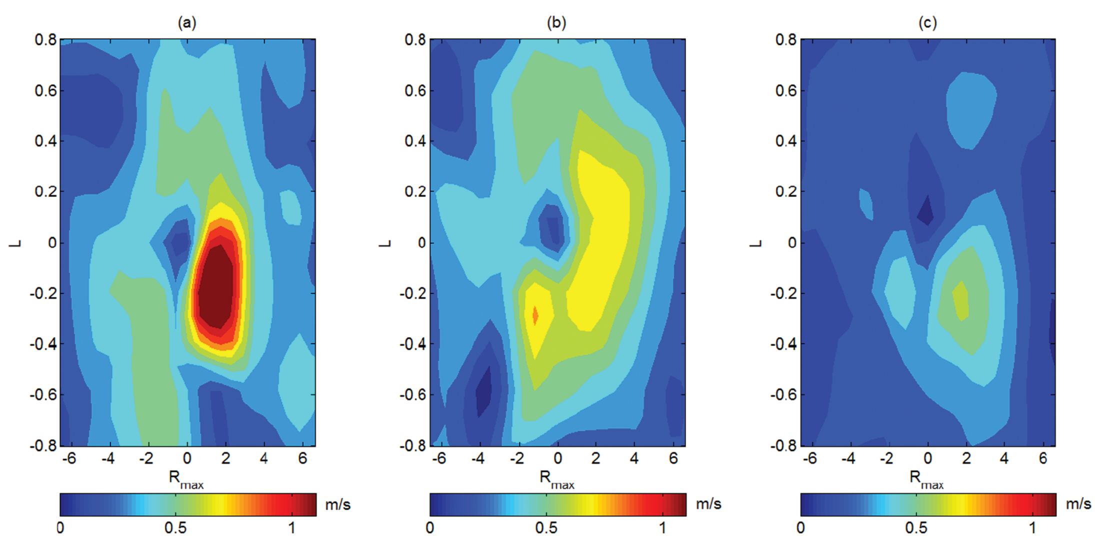

Figure 6. Mean current speed (m s^{-1}) under (a) category-4 and -5, (b) category-2 and -3, and (c) tropical storm and category-1 TCs with the slow ($F_r < 1$) translation speed. Contour interval is 0.1 m s^{-1}.

category-4 and -5, category-2 and -3, and TS and category-1 TCs, with the color contour showing the current speeds. These velocity fields have strongly left-to-right asymmetric distributions with pronounced velocity maximum of 1.1 m s^{-1}, 0.7 m s^{-1}, and 0.5 m s^{-1}. This result also provides the characterization of the near-surface velocity response to category-4 and -5 TCs in terms of a relatively long time series of direct velocity measurements. For all the TC intensity levels, the distances between the velocity maximum and storm center are approximately $2R_{\max}$. The

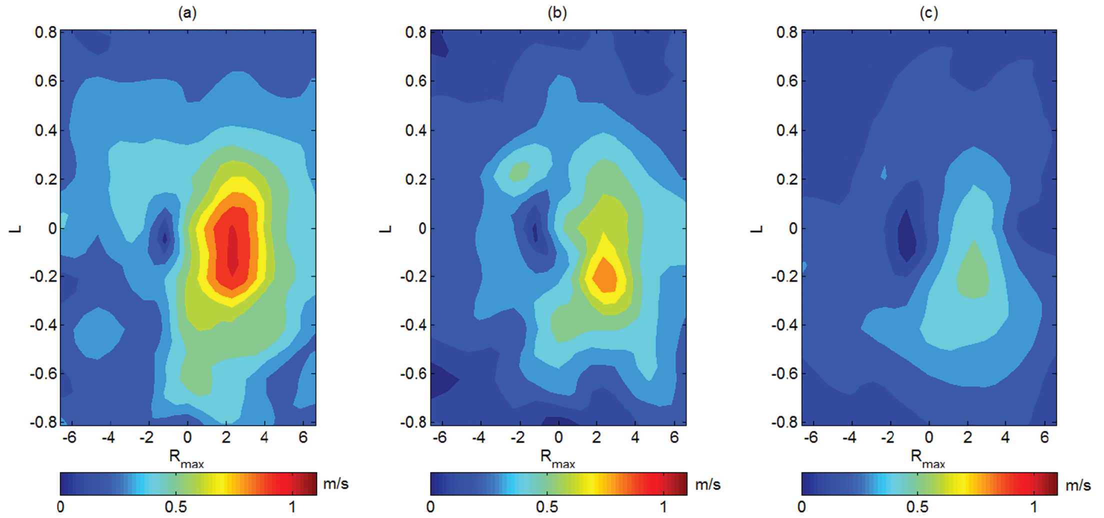

Figure 7. Mean current speed (m s^{-1}) under (a) category-4 and −5, (b) category-2 and −3, and (c) tropical storm and category-1 TCs with the fast ($1 \leqq F_r < 2$) translation speed. Contour interval is 0.1 m s^{-1}.

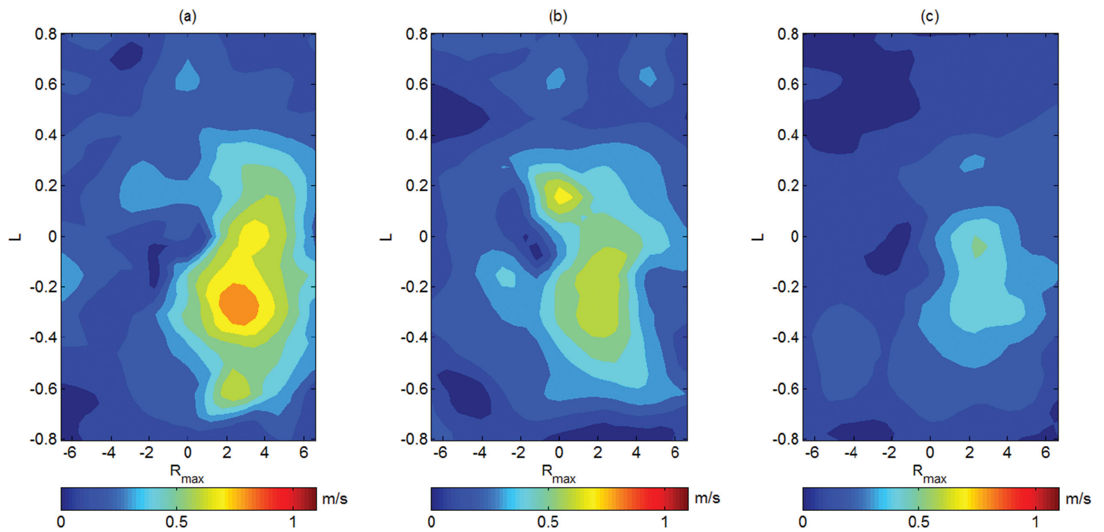

Figure 8. Mean current speed (m s^{-1}) under (a) category-4 and −5, (b) category-2 and −3, and (c) tropical storm and category-1 TCs with the fastest ($F_r \geqq 2$) translation speed. Contour interval is 0.1 m s^{-1}.

location of the velocity maximum depends on the speed of the storm and is not always $2R_{\max}$ from theory. The asymmetry of the observed velocity fields also agree with the previous studies [*Price*, 1981; *Price et al.*, 1994; *Chu et al.*, 2000]. The left-to-right asymmetry in current amplitude is mainly due to the resonant coupling between clockwise-rotating wind stress and near-inertial currents on the right side of a storm (in the northern hemisphere). Also note that the strongest wind stress occurs in this side of the storm.

Table 1. Rate of Occurrence of Three F_r Ranges in the Three Storm Groups

	Moving Speed	Category-4 and −5 (%)	Category-2 and −3 (%)	Category-1 and Tropical Storm (%)
$F_r < 1$	Slow	18	28	23
$1 \leqq F_r < 2$	Fast	53	45	48
$F_r \geqq 2$	Fastest	29	27	29

4. Discussion

[13] The ratio between the translation speed of the storm U_h and the phase speed of the first baroclinic mode c_1 determines whether the upper-ocean response is in the form of upwelling or near-inertial wave wakes [*Geisler*, 1970; *Nilsson*, 1995]. If $U_h >> c_1$ ($F_r >> 1$), the near-inertial waves are the dominant feature of the baroclinic response. For $U_h \geqq c_1$ ($F_r \geqq 1$), the wake is changed into a perturbation on a smooth pattern of upwelling. For $U_h < c_1$ ($F_r < 1$), there is no wake. To evaluate the near-inertial velocity response over the northwestern Pacific, consider a two-layer approach in which c_1 is given by

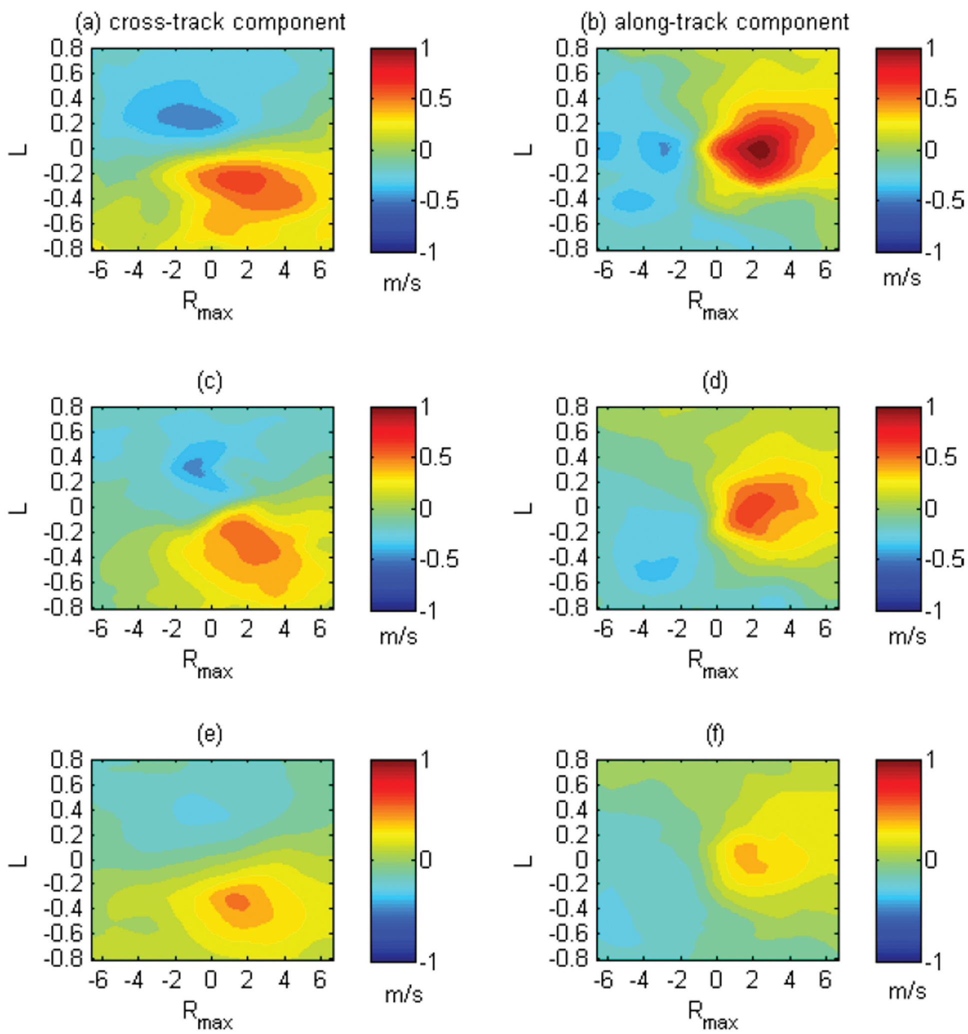

Figure 9. Along-track and cross-track observed current components (m s^{-1}) under fast moving ($1 \leqq F_r < 2$) (a, b) category-4 and −5 TCs, (c, d) category-2 and −3 TCs, and (e, f) tropical storm and category-1 TCs. Contour interval is 0.1 m s^{-1}.

$$c_1{}^2 = g\frac{(\rho_2 - \rho_1)h_1 h_2}{\rho_2(h_1 + h_2)}, \tag{6}$$

where h_1 is 18°C isotherm depth, h_2 is the thickness of the layer extending from h_1 down to 1000 m (i.e., $h_2 = 1000 - h_1$), and ρ_1 and ρ_2 are vertically averaged densities in upper and lower layers [*Jaimes and Shay*, 2009]. The climatological (summer) world ocean atlas (WOA) temperature and salinity profiles from the NOAA National Oceanography Data Center (NODC) (http://www.nodc.noaa.gov/OC5/WOA09/pr_woa09.html) were used to calculate h_1, ρ_1, and ρ_2 at each grid point in the North Pacific. The calculated mean values of c_1 during summer were ~2.88 m s^{-1} in the study area (Figure 5).

[14] In order to show the observed current fields under slow- and fast-moving storms using direct velocity measurements, the critical limit F_r was used to separate storms into the "slow," "fast," and "fastest" categories. Different responses of near-surface current vectors were found under slow ($F_r < 1$) (Figure 6), fast ($1 \leqq F_r < 2$) (Figure 7), and fastest ($F_r \geqq 2$) (Figure 8) moving TCs with all the intensity levels. For slow-moving TCs ($F_r < 1$), the mean ocean current fields show a similar pattern of upwelling (Figure 6). For fast ($1 \leqq F_r < 2$, Figure 7)-moving TCs, the mean ocean current fields show a similar wake in the rear area of storm center. For fastest ($F_r \geqq 2$, Figure 8)-moving TCs, mean ocean current fields are also show the upper-ocean velocity response is in the form of wave wakes. This rightward bias of OML velocity occurs because wind stress turns clockwise (inertially) with time on the right side of the track and anticlockwise on the left side [*Chang and Anthes*, 1978; *Price*, 1981]. For typical storm sizes and translation speeds, the rate of wind stress turning is *O*(*f*) [*Price*, 1983]. As U_h exceeds c_1 ($F_r > 1$), the theoretically predicted baroclinic response driven by near-inertial current [*Geisler*, 1970] consists of the ocean velocity field observed under fast-moving storms. With this theory, the wake of a moving disturbance fills a wedge in the lee of the storm. Thus, our results roundly agree with Geisler's theory at all TC intensity levels using direct velocity measurements. It is noted that U_h of a storm is not a constant in reality. Table 1 shows the rate of occurrence of three F_r

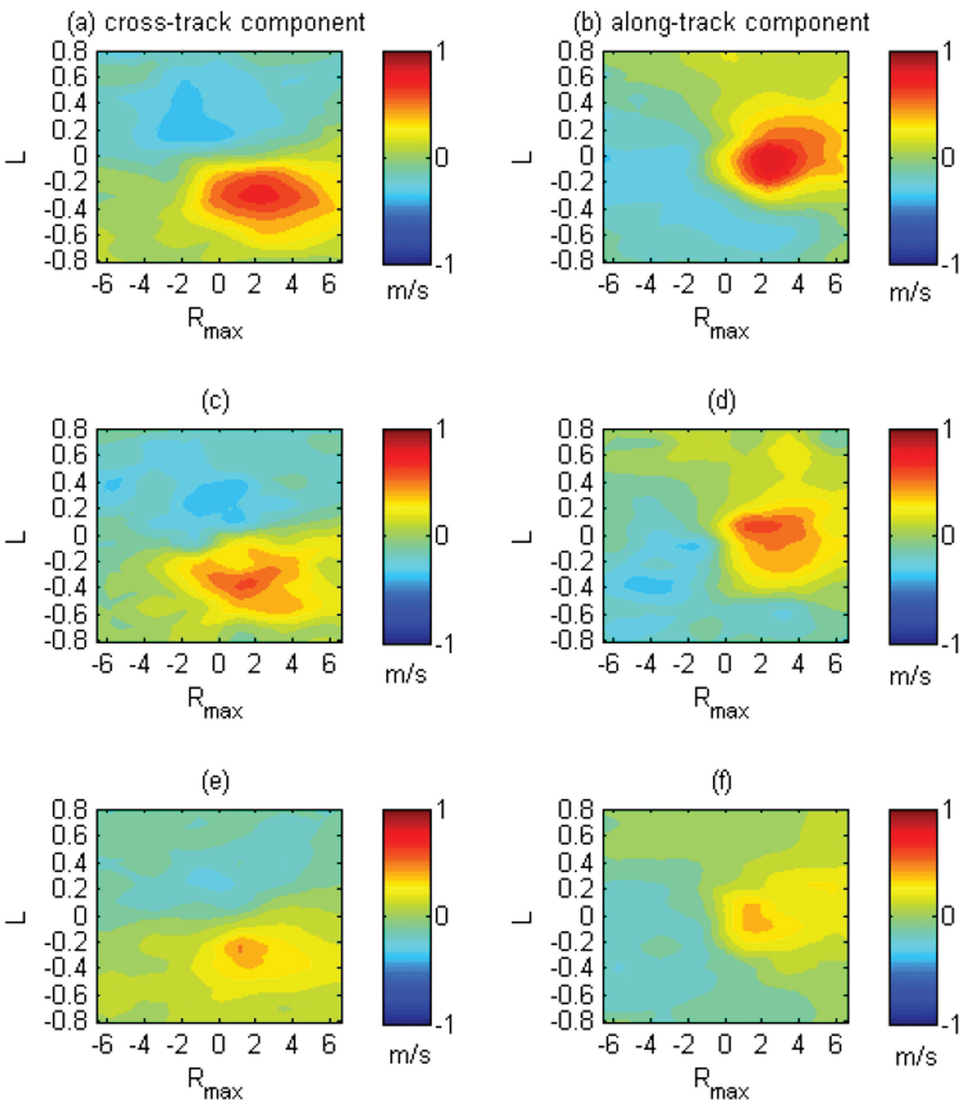

Figure 10. Along-track and cross-track observed current components (m s^{-1}) under fastest moving ($F_r \geqq 2$) (a, b) category-4 and −5 TCs, (c, d) category-2 and −3 TCs, and (e, f) tropical storm and category-1 TCs. Contour interval is 0.1 m s^{-1}.

ranges for the three storm groups. The range of $1 \leqq F_r < 2$ most often occur for all the three storm groups (category-4 and −5 TCs: 53%, category-2 and −3 TCs: 45%, and TS and category-1 TCs: 43%). For typical storm sizes and translation speeds (i.e., under the condition: $1 \leqq F_r < 2$), the rate of wind stress turning is $O(f)$ [*Price*, 1983]. Since the wind-driven near-inertial current decays in several days [*Gill*, 1984], a few components of near-inertial velocity, which were induced by previous storm with a fast (typical) U_h, could switch to the velocity pattern under a slow ($F_r < 1$)-moving storm (Figure 6), with a little perturbation of near-inertial current from a pattern of upwelling, but the overall velocity patterns still agree roughly with the Geisler's theory. Recent study [*Mei et al.*, 2012] indicates that U_h of category-5 hurricanes is around 1 m s^{-1} faster than TSs. Table 1 shows slowly moving storms ($F_r < 1$) are fewer in category-4 and −5 (18%) than in weaker storms (23 and 28%). Therefore, our data here roughly agrees with the result of *Mei et al*. [2012].

[15] Our observations also verify earlier modeling results. Figures 9 and 10 show the mean cross-track and along-track components of observed OML velocity under fast ($1 \leqq F_r < 2$)- and fastest ($F_r \geqq 2$)-moving storms, respectively. The patterns of cross-track and along-track components of velocity fields in Figures 9 and 10 are very similar to the previous model-predicted [*Price*, 1981] and parameterized [*Price*, 1983] OML velocity fields under a moving storm in the first inertial period ($-0.5P_I < t < 0.5P_I$) or wavelength of storm ($-0.5L < Y < 0.5L$), and the cross-track component lags the along-track component by approximately one-quarter inertial period or wavelength of storm in observations (Figures 9 and 10). The expected velocity response in the OML to a moving TC is estimated by a wind-driven horizontal velocity parameter U_s [*Price*, 1983; *Price et al*., 1994; *Jaimes and Shay*, 2009],

$$U_s = \frac{\tau R_{\max}}{h U_h}, \tag{7}$$

Table 2. Comparison Between the Observed Wind-Driven Velocity U_e From Drifter and the Scaled Wind-Driven Velocity U_s

Parameter	Category-4 and −5	Category-2 and −3	Category-1 and TS
W	60 m s^{-1}	45 m s^{-1}	30 m s^{-1}
τ	6.6 N m^{-2}	4.3 N m^{-2}	2.2 N m^{-2}
U_s	1.2 m s^{-1}	0.8 m s^{-1}	0.4 m s^{-1}
U_e	1.1 m s^{-1}	0.7 m s^{-1}	0.5 m s^{-1}

where $\tau = |\tau| = \sqrt{(\tau^x)^2 + (\tau^y)^2}$ and h is the OML depth. For a typical storm in the Pacific, $h = 50$ m (Figure 5b), $U_h = 4.9$ m s^{-1}, $R_{\max} = 47$ km in the study area averaged over all storms (1985–2009) [*Hsu and Yana*, 1998]. The surface wind stress (τ)

$$\tau = \rho_{\text{air}} C_d W^2, \tag{8}$$

is often used by oceanographers. Here, ρ_{air} is the air density, C_d is the drag coefficient, and W is the wind speed at a reference height (usually 10 m). Typically for air, the density ρ_{air} is about 1.22 kg m^{-3} [*Zedler*, 2009], and the C_d value used is in the type taken from *Powell et al*. [2003] (*after Zedler et al*. [2009]). Then, the estimated wind stress under category-4 and −5, category-2 and −3, and TS and category-1 TCs can be calculated from the wind speeds of 60, 45, and 30 m s^{-1} (Table 2). Thus, the OML wind-driven horizontal velocities U_s under category-4 and −5, category-2 and −3, and TS and category-1 TCs are 1.2, 0.8, and 0.4 m s^{-1}, respectively. These scaled OML wind-driven velocities U_s are similar as the observed wind-driven velocities $U_e(= |U_e|)$ in Figure 5 (1.1, 0.7, and 0.5 m s^{-1}) from SVP drifter (Table 2). The patterns and magnitudes of the observed velocities from drifters both confirm with them of OML wind-driven horizontal velocity U_s.

5. Summary

[16] Flow patterns of strong near-surface currents under all TC intensity levels in the northwestern Pacific have been illustrated entirely from SVP drifter measurements. Near-surface current speeds in excess of 2.0 m s^{-1} have been observed in these category-4 and −5 TCs. The mean velocity maximums of 1.1 m s^{-1}, 0.7 m s^{-1}, and 0.5 m s^{-1} were present to the right of the path of the storm center under category-4 and −5, category-2 and −3, and TS and category-1 TCs, respectively. This study successfully shows the characterization of the near-surface velocity response to all recorded TCs and roughly agrees the Geisler's theory after separating storms into slow ($F_r < 1$), fast ($1 \leqq F_r < 2$), and fastest ($F_r \geqq 2$) categories, with relatively long time periods (1985–2009) of direct velocity measurements. Our observations also verify earlier modeling results of *Price* [1983].

[17] **Acknowledgments.** This research was completed with grants from Aim for the Top University Plan from the Ministry of Education (00C030200) and National Science Council (NSC100–2611-M-110-004) of Taiwan, Republic of China. P.C.C. was supported by the Naval Oceanographic Office. We are grateful for the comments of two anonymous reviewers.

References

Alford, M. H. (2001), Internal swell generation: The spatial distribution of energy flux from the wind to mixed-layer near-inertial motions, *J. Phys. Oceanogr.*, *31*, 2359–2368.

Alford, M. H. (2003), Improved global maps and 54-year history of wind-work on ocean inertial motions, *J. Geophys. Res.*, *30*(8), 1424, doi:10.1029/2002GL016614.

Black, P. G., R. L. Elsberry, L. K. Shay, R. Partridge, and J. Hawkins (1988), Hurricane Josephine surface winds and ocean response determined from air-deployed drifting buoys and concurrent research aircraft data, *J. Atmos. Oceanic Technol.*, *5*, 683–698.

Brink, K. H. (1989), Observations of the response of thermocline currents to a hurricane, *J. Phys. Oceanogr.*, *19*, 1017–1022.

Brooks, D. A. (1983), The wake of Hurricane Allen in the western Gulf of Mexico, *J. Phys. Oceanogr.*, *13*, 117–129.

Centurioni, L. R., and P. P. Niiler (2003), On the surface currents of the Caribbean Sea, *Geophys. Res. Lett.*, *30*(6), 1279, doi:10.1029/2002GL016231.

Centurioni, L. R., P. P. Niiler, and D. K. Lee (2004), Observations of inflow of Philippine sea surface water into the South China sea through the Luzon strait, *J. Phys. Oceanogr.*, *34*, 113–121.

Chang, S., and R. Anthes (1978), Numerical simulations of the ocean's nonlinear baroclinic response to translating hurricanes, *J. Phys. Oceanogr.*, *8*, 468–480.

Chang, S. W. (1985), Deep ocean response to hurricanes as revealed by an ocean model with free surface. Part I: Axisymmetric case, *J. Phys. Oceanogr.*, *15*, 1847–1858.

Chang, Y.-C., R.-S. Tseng, and L. R. Centurioni (2010), Typhoon-induced strong surface flows in the Taiwan Strait and Pacific, *J. Oceanogr.*, *66*, 175–182.

Chu, P. C., J. M. Veneziano, and C. W. Fan (2000), Response of the South China Sea to tropical cyclone Ernie 1996, *J. Geophys. Res.*, *105*, 13,991–14,009.

D'Asaro, E. A. (1985), The energy flux from the wind to near-inertial motions in the surface mixed layer, *J. Phys. Oceanogr.*, *15*, 1043–1059.

Freeland, H. J. (1975), Statistical observations of the trajectory of neutrally buoyant floats in the North Atlantic, *J. Mar. Res.*, *33*, 383–404.

Garrett, C., and W. H. Munk (1972), Space-time scales of internal waves, *Geophys. Fluid Dyn.*, *2*, 225–264.

Geisler, J. E. (1970), Linear theory of the response of a two-layer ocean to a moving hurricane, *Geophys. Fluid Dyn.*, *1*, 249–272.

Gill, A. E. (1984), On the behavior of internal waves in the wake of storms, *J. Phys. Oceanogr.*, *14*, 1129–1151.

Ginis, I., and G. Sutyrin (1995), Hurricane-generated depth-averaged currents and sea surface elevation, *J. Phys. Oceanogr.*, *25*, 1218–1242.

Greatbatch, R. J. (1984), On the response of the ocean to a moving storm: Parameters and scales, *J. Phys. Oceanogr.*, *14*, 59–78.

Hsu, S. A., and Z. Yana (1998), A note on the radius of maximum winds for hurricanes, *J. Coastal Res.*, *12*, 667–668.

Jacob, S. D., and L. K. Shay (2003), The role of oceanic mesoscale features on the tropical cyclone-induced mixed layer response: A case study, *J. Phys. Oceanogr.*, *33*, 649–676.

Jaimes, B., and L. K. Shay (2009), Mixed layer cooling in mesoscale oceanic eddies during hurricanes Katrina and Rita, *Mon. Weather Rev.*, *137*, 4188–4207.

Jaimes, B., and L. K. Shay (2010), Near-inertial wave wake of hurricanes Katrina and Rita over mesoscale oceanic eddies, *J. Phys. Oceanogr.*, *40*, 1320–1337.

Kunze, E. (1985), Near-inertial wave propagation in geostrophic shear, *J. Phys. Oceanogr.*, *15*, 544–565.

Lee, D.-K., and P. P. Niiler (2005), The energetic surface circulation patterns of the Japan/East Sea, *Deep-Sea Res. II*, *52*, 1547–1563.

Lin, I.-I, W. T. Liu, C.-C. Wu, J. C. H. Chiang, and C.-H. Sui (2003a), Satellite observations of modulation of surface winds by typhoon-induced upper ocean cooling, *Geophys. Res. Lett.*, *30*(3), 1131, doi:10.1029/2002GL015674.

Lin, I., W. T. Liu, C.-C. Wu, G. T. F. Wong, C. Hu, Z. Chen, W.-D. Liang, Y. Yang, and K.-K. Liu (2003b), New evidence for enhanced ocean primary production triggered by tropical cyclone, *Geophys. Res. Lett.*, *30*(13), 1718, doi:10.1029/2003GL017141.

Liu, L. L., W. Wang, and R. X. Huang (2008), The mechanical energy input to the ocean induced by tropical cyclones, *J. Phys. Oceanogr.*, *38*, 1253–1266.

Mei, W., C. Pasquero, and F. Primeau (2012), The effect of translation speed upon the intensity of tropical cyclones over the tropical ocean, *Geophys. Res. Lett.*, *39*, L07801, doi:10.1029/2011GL050765.

Mitchell, D. A., W. J. Teague, E. Jarosz, and D. W. Wang (2005), Observed currents over the outer continental shelf during Hurricane Ivan, *Geophys. Res. Lett.*, *32*, L11610, doi:10.1029/2005GL023014.

Mooers, C. N. K. (1975), Several effects of a baroclinic current on the cross-stream propagation of inertial-internal waves, *Geophys. Fluid Dyn.*, *6*, 245–275.

Niiler, P. P. (2001), The world ocean surface circulation, *in Ocean Circulation and Climate: Observing and Modeling the Global Ocean*, *Int. Geophys. Ser.*, vol. *77*, pp. 193–204, edited by G. Siedler, J. Church, and J. Gould, Academic Press, San Diego, Calif.

Niiler, P. P., A. S. Sybrandy, K. Bi, P. M. Poulain, and D. Bitterman (1995), Measurements of the water following capability of holey-sock and TRISTAR drifters, *Deep-Sea Res. A*, *42*, 1951–1964.

Nilsson, J. (1995), Energy flux from traveling hurricanes to the oceanic internal wave field, *J. Phys. Oceanogr.*, *25*, 558–573.

O'Brien, J. J., and R. O. Reid (1967), The non-linear response of a two-layer baroclinic ocean to a stationary, axially-symmetric hurricane: Part I. Upwelling induced by momentum transfer. *J. Atmos. Sci.*, *24*, 197–207.

Olbers, D. J. (1981), The propagation of internal waves in a geostrophiccurrent, *J. Phys. Oceanogr.*, *11*, 1224–1233.

Powell, M., P. Vickery, and T. Reinhold (2003), Reduced drag coefficients for high wind speeds in tropical cyclones, *Nature*, *422*, 279–283.

Price, J. F. (1981), Upper ocean response to a hurricane, *J. Phys. Oceanogr.*, *11*, 153–175.

Price, J. F. (1983), Internal wave wake of a moving storm. Part I: Scales, energy budget and observations, *J. Phys. Oceanogr.*, *13*, 949–965.

Price, J. F., T. B. Sanford, and G. Z. Forristall (1994), Forced stage response to a moving hurricane, *J. Phys. Oceanogr.*, *24*, 233–260.

Sanford, T. B., J. F. Price, and J. B. Girton (2011), Upper-ocean response to hurricane Frances (2004) observed by profiling EM-APEX floats, *J. Phys. Oceanogr.*, *41*, 1041–1056.

Shay, L. K., and S. W. Chang (1997), Free surface effects on the near-inertialocean current response to a hurricane: A revisit, *J. Phys. Oceanogr.*, *27*, 23–39.

Shay, L. K., and R. L. Elsberry (1987), Near-inertial ocean current response to Hurricane Frederic, *J. Phys. Oceanogr.*, *17*, 1249–1269.

Shay, L. K., R. L. Elsberry, and P. G. Black (1989), Vertical structure of the ocean current response to a hurricane, *J. Phys. Oceanogr.*, *19*, 649–669.

Sriver, R. L., and M. Huber (2007), Observational evidence for an ocean heat pump induced by tropical cyclones, *Nature*, *447*, 577–580.

Teague, W. J., E. Jarosz, D. W. Wang, and D. A. Mitchell (2007), Observed oceanic response over the upper continental slope and outer shelf during Hurricane Ivan, *J. Phys. Oceanogr.*, *37*, 2181–2206.

Wang, W., and R. X. Huang (2004), Wind energy input to the surface waves, *J. Phys. Oceanogr.*, *34*, 1276–1280.

Weller, R. A. (1982), The relation of near-inertial motions observed in the mixed layer during the JASIN (1978) experiment to thelocal wind stress and to the quasi-geostrophic flow field, *J. Phys. Oceanogr.*, *12*, 1122–1136.

Wunsch, C. (1998), The work done by the wind on the oceanic general circulation, *J. Phys. Oceanogr.*, *28*, 2332–2340.

Zedler, S. E. (2009), Simulations of the ocean response to a hurricane: Nonlinear processes, *J. Phys. Oceanogr.*, *39*, 2618–2634.

Zedler, S. E., P. P. Niiler, D. Stammer, E. Terrill, and J. Morzel (2009), Ocean's response to Hurricane Frances and its implications for drag coefficient parameterization at high wind speeds, *J. Geophys. Res.*, *114*, C04016, doi: 10.1029/2008JC005205.

Zheng, Q., R. J. Lai, N. E. Huang, J. Pan, and W. T. Liu (2006), Observation of ocean current response to 1998 Hurricane Georges in the Gulf of Mexico, *Acta Oceanol. Sin.*, *25*, 1–15.